

# Localized Rayleigh Instability in Evaporation Fronts

Haim Diamant<sup>1,2</sup> and Oded Agam<sup>2,\*</sup>

<sup>1</sup>*School of Chemistry, Sackler Faculty of Exact Sciences, Tel Aviv University, Tel Aviv 69978, Israel*

<sup>2</sup>*The Racah Institute of Physics, The Hebrew University, Jerusalem 91904, Israel*

(Dated: March 22, 2019)

A qualitatively different manifestation of the Rayleigh instability is demonstrated, where, instead of the usual extended undulations and breakup of the liquid into many droplets, the instability is localized, leading to an isolated narrowing of the liquid filament. The localized instability, caused by a nonuniform curvature of the liquid domain, plays a key role in the evaporation of thin liquid films off solid surfaces.

PACS numbers: 68.15.+e, 68.03.Kn, 68.08.Bc

The Rayleigh instability of slender liquid bodies, driven by surface tension, is part of everyday experience and has been systematically studied for well over a century [1, 2]. Its manifestations are diverse, ranging from the breakup into droplets of inviscid, viscous, and viscoelastic liquid jets and bridges [1] to the pearling of fluid membranes [3]. The liquid bodies considered in earlier studies were usually translation-invariant along their long dimension, resulting in unstable modes which were extended [1, 2] or had a steadily propagating front [4]. The propagation of forced perturbations from a fixed nozzle were studied as well [1]. In this Letter we investigate a qualitatively different scenario of the Rayleigh instability, in which the translation invariance is broken by a nonuniform curvature, and show that the fastest-growing mode of this instability is localized. The localization is reminiscent of the problem of a quantum particle moving inside a curved stripe [5, 6]. When the latter system is transformed into an effective one-dimensional problem, an attractive potential emerges, whose minimum is located at the point of maximum curvature, giving rise to bound (localized) states.

Thin liquid bodies are abundant in phenomena related to wetting of solid substrates [2, 7]. Two processes are particularly relevant to the current work: (i) the dewetting of a nonvolatile, nonwetting film [2, 8, 9]; and (ii) the evaporation of a volatile, totally wetting film [10–13]. Both processes exhibit the kinetics of a first-order transition, where dry domains [in (i)], or domains covered by a molecularly thin liquid [in (ii)], nucleate and grow into a much thicker film. Importantly, in both processes the dewetting front has a long, slender rim of excess fluid [2]. The growing domains may have a stable circular boundary [8, 10] or evolve through elaborate instabilities and patterns [10–14]. An analogy has recently been drawn between the pattern formation in the volatile case and Saffman-Taylor viscous fingering in a Hele-Shaw cell having a time-varying thickness [15]. The additional dynamics of the liquid rim at the domain boundary, however, crucially affects the selection of patterns in experiments, e.g., the doublon pattern shown in Fig. 1, which is uncommon in Saffman-Taylor fingering [11, 15].

We model the droplet’s rim as a long, curved liquid strip of uniform width  $w$ . It is parametrized using the locally orthogonal triad  $(s, u, z)$  as depicted in Fig. 2, where  $u \in [-w/2, w/2]$  and  $z \in [0, h]$ ,  $h(s, u)$  being the local liquid height. The rim is in contact with the wet and dry domains at  $u = -w/2$  and  $w/2$ , respectively. The local curvature of the centerline  $(s, 0, 0)$  is denoted by  $\kappa(s)$  and taken as positive when the rim curves away from the dry domain. (In Fig. 2  $\kappa < 0$ .) We assume separation of time scales between the growth of the finger and the faster development of the rim instability, as observed in the evaporation experiments. Thus, although the rim itself is a dynamic effect,  $w$  and  $\kappa(s)$  can be taken as time-independent.

Within the lubrication approximation ( $|\nabla h| \ll 1$ ) [16], the equation of motion for the liquid is

$$\partial_t h = -\nabla \cdot \mathbf{j}, \quad \mathbf{j} = -\frac{h^3}{3\eta} \nabla p, \quad (1)$$

where  $p$  is the liquid pressure,  $\eta$  its viscosity, and spa-

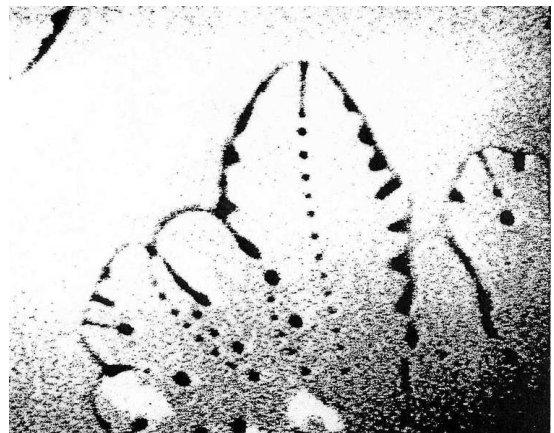


FIG. 1: Doublon patterns observed in the evaporation of water off a clean mica surface [17]. Fingers of a molecularly thin water film grow into a thicker film. A local indentation at the finger tip leads to splitting and the formation of a liquid spine that subsequently breaks into droplets. The fingers are hundreds  $\mu\text{m}$  wide.

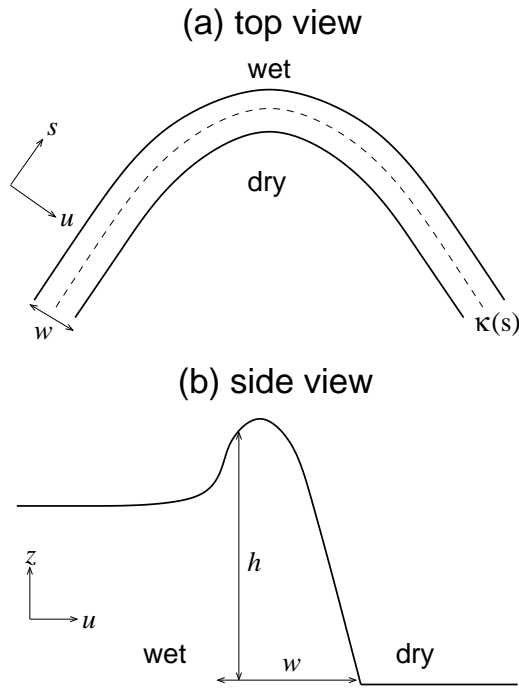


FIG. 2: Schematic view of the system and its parametrization. A curved liquid rim of uniform width  $w$ , nonuniform curvature  $\kappa(s)$ , and height profile  $z = h(s, u)$ , lies at the interface between a thick liquid film (wet domain) and a much thinner one (dry domain).

tial derivatives are in the  $(s, u)$  plane. In  $p$  we include contributions from the Laplace pressure and disjoining pressure  $\Pi(h)$  (i.e., surface interactions) [7],

$$p = -\gamma \nabla^2 h - \Pi(h), \quad (2)$$

where  $\gamma$  is the surface tension of the liquid. Substituting in Eqs. (1) and (2) a small perturbation of the steady profile,  $h = h_0 + \psi$ , linearizing in  $\psi$ , and neglecting spatial derivatives of  $h_0$ , we obtain

$$\partial_t \psi = \hat{O} \psi, \quad \hat{O} = -\Gamma_0 q_0^{-4} (\nabla^4 + 2q_0^2 \nabla^2). \quad (3)$$

In Eq. (3) the Laplacian is given by [6]

$$\begin{aligned} \nabla^2 &= g^{-1/2} \partial_s g^{-1/2} \partial_s + g^{-1/2} \partial_u g^{1/2} \partial_u, \\ g(s, u) &= [1 + u \kappa(s)]^2, \end{aligned} \quad (4)$$

and the following length and time scales appear:

$$q_0^{-1} = [2\gamma/\Pi'(h_0)]^{1/2}, \quad \Gamma_0^{-1} = 12\eta\gamma/(h_0^3[\Pi'(h_0)]^2). \quad (5)$$

In the systems under consideration the disjoining pressure is usually governed by van der Waals interactions [7], whereby  $\Pi' = H/(2\pi h_0^4)$ ,  $H \sim 10^{-13}$  erg being the Hamaker constant. The length  $b = (H/\gamma)^{1/2}$  is invariably of molecular scale,  $\sim 1$  nm. Hence, the value of  $q_0^{-1} \sim h_0^2/b$  is primarily determined by the rim thickness,

$h_0$ , which has very different values in the dewetting and evaporation processes. In the dewetting case of Ref. [8]  $h_0$  is about  $50 \mu\text{m}$ , leading to  $q_0^{-1}$  of order meters and an unphysically long  $\Gamma_0^{-1}$ . In the evaporation process of Ref. [12], by contrast,  $h_0$  is of order 10 nm, yielding  $q_0^{-1}$  of micron scale and  $\Gamma_0^{-1}$  of order  $10^{-2}$  s (though the latter is highly sensitive to the thickness). The rim width,  $w$ , is of mm scale in both cases; thus,  $wq_0 \ll 1$  for the dewetting case, and  $wq_0 \gg 1$  for the evaporation one. As we shall presently see, instability of the rim requires  $wq_0 \gtrsim 1$ , which clarifies the strikingly different dynamics observed in the two processes.

A key feature of the system is that the rim separates domains of differing properties (Fig. 2). This implies asymmetric boundary conditions at  $u = \pm w/2$  and, consequently, sensitivity of the results to the curvature direction (sign of  $\kappa$ ). At the boundary with the thick liquid film we impose a fixed height and a vanishing surface curvature,

$$u = -w/2: \quad \psi = 0, \quad \nabla^2 \psi = 0, \quad (6)$$

thus ensuring that the pressure [Eq. (2)] changes continuously between the rim and the film [18]. At the boundary with the dry domain we assume a fixed contact angle and a vanishing outward current,

$$u = w/2: \quad \partial_u \psi = 0, \quad \partial_u \nabla^2 \psi = 0. \quad (7)$$

The operator  $\hat{O}$ , as defined by Eq. (3) and the boundary conditions (6) and (7), is hermitian. In general it does not commute with the Laplacian because of the spatially varying  $g(s, u)$ . In cases where  $\hat{O}$  and  $\nabla^2$  do commute, the spectrum of  $\hat{O}$  (denoted by  $\Gamma$ ) can be written in terms of that of  $\nabla^2$  ( $\lambda$ ) as  $\Gamma = -\Gamma_0 q_0^{-4} \lambda(\lambda + 2q_0^2)$ , and is thus bounded from above by  $\Gamma_0$ . Hence, in such cases the fastest growing mode has (at the most) a rate  $\Gamma_0$  as given by Eq. (5).

In the simple case of a straight rim [13],  $\kappa \equiv 0$ , we have  $[\hat{O}, \nabla^2] = 0$ . The eigenmodes of  $\hat{O}$  in this case are extended,

$$\psi_{nq} = A e^{iqs + \Gamma_{nq} t} \sin[k_n(u + w/2)], \quad (8)$$

where  $A$  is an arbitrary amplitude,  $q$  the wavenumber along the rim,  $k_n = \pi(n - 1/2)/w$  ( $n = 1, 2, \dots$ ) the wavenumber in the transverse direction, and

$$\Gamma_{nq} = \Gamma_0 (q^2 + k_n^2) [2q_0^2 - (q^2 + k_n^2)] / q_0^4 \quad (9)$$

is the growth rate. Unstable modes, having  $\Gamma_{nq} > 0$ , are obtained for a sufficiently wide rim,  $wq_0 > \pi/(2\sqrt{2})$ ; getting fastest growing modes of finite wavelength requires the slightly stricter condition  $wq_0 > \pi/2$ . These modes have wavenumbers  $q_n = (q_0^2 - k_n^2)^{1/2}$  and the maximum growth rate  $\Gamma = \Gamma_0$ . In the case of a circular rim of fixed curvature,  $\kappa \equiv \kappa_0 \neq 0$ , despite the nonuniform metric  $g = (1 + \kappa_0 u)^2$ ,  $\hat{O}$  and  $\nabla^2$  still commute due to

rotational symmetry. Hence, a finite uniform curvature cannot accelerate the instability beyond the rate  $\Gamma_0$ .

We now address the interesting and practically relevant case of a nonuniform curvature  $\kappa(s)$ . Motivated by the evaporation experiments (Fig. 1 and [10–13]) and inspired by the quantum bound states (i.e., localized eigenmodes of  $\nabla^2$ ) found in a similar curved geometry [6], we look for a localized unstable mode of  $\hat{O}$ , whose growth rate exceeds  $\Gamma_0$ . To this end we employ a variational approach, which sets a lower bound for the maximum rate according to

$$\Gamma_{\max} \geq \bar{\Gamma}[\psi] \equiv \langle \psi | \hat{O} | \psi \rangle / \langle \psi | \psi \rangle, \quad (10)$$

$\psi(s, u)$  being any trial function that satisfies the boundary conditions (6) and (7).

For a general form of  $\kappa(s)$  it is difficult to construct a good variational wavefunction which will satisfy the boundary conditions. To simplify the analysis we assume that the curvature is both small and slowly varying in space. In this regime the wavefunction may be locally approximated by that of a circular rim having curvature  $\kappa(s)$ . This observation leads to the following choice of variational wavefunction:

$$\psi(s, u) = A\phi(s, u)e^{iq_1s}e^{-s^2/a^2}, \quad (11)$$

where

$$\begin{aligned} \phi(s, u) = & \left\{ 1 - \kappa(s)\frac{w}{\pi}\left[k_1\left(u + \frac{w}{2}\right) - \frac{2}{\pi}\right] \right\} \sin\left[k_1\left(u + \frac{w}{2}\right)\right] \\ & - \left[ 2\kappa(s)\frac{w}{\pi^2}k_1\left(u + \frac{w}{2}\right) \right] \cos\left[k_1\left(u + \frac{w}{2}\right)\right]. \end{aligned} \quad (12)$$

Here  $k_1 = \pi/(2w)$ ,  $q_1 = (q_0^2 - k_1^2)^{1/2}$ , and the localization length  $a$  serves as a variational parameter [19, 20]. Equation (12) has been obtained from the asymptotic form of the eigenmodes for a circular rim in the limit of small curvature, while replacing  $\kappa_0$  with the slowly varying curvature,  $\kappa(s)$ . For the sake of concreteness let us take

$$\kappa(s) = \kappa_0 e^{-s^2/\sigma^2}. \quad (13)$$

Our calculation is performed to leading order in two small parameters:  $\delta = \kappa_0 w$  and  $\epsilon = (q_1 a)^{-1}$ . (Note that the overall turn of the rim,  $\kappa_0 \sigma$ , may still be appreciable.) The smallness of  $\epsilon$ , implying that the localized mode extends many wavelengths away from the tip, is an ansatz to be confirmed below. In addition, we assume  $q_0 w \gg 1$  (and thus  $q_1 w \gg 1$ ) to be safely inside the unstable regime. The trial function of Eqs. (11) and (12) satisfies the boundary conditions for  $\psi(-w/2)$  and  $\partial_u \psi(w/2)$  exactly, while those for  $\nabla^2 \psi(-w/2)$  and  $\partial_u \nabla^2 \psi(w/2)$  are violated only at the orders  $\delta^2$  and  $\delta \epsilon^2$ , respectively.

Within this approximation we obtain from Eq. (10)

$$\bar{\Gamma}(a) = \Gamma_0 \left[ 1 - 4\frac{q_1^2}{q_0^4} \left( \frac{1}{a^2} + \frac{\sqrt{2}\kappa_0\sigma}{wa} \right) \right]. \quad (14)$$

Maximizing  $\bar{\Gamma}$  with respect to  $a$  yields

$$\begin{aligned} a^* &= -\sqrt{2}w/(\kappa_0\sigma) \\ \Gamma_{\max} &\geq \bar{\Gamma}(a^*) = \Gamma_0 \left( 1 + \frac{2q_1^2\kappa_0^2\sigma^2}{q_0^4w^2} \right). \end{aligned} \quad (15)$$

Thus, provided that the rim is negatively curved ( $\kappa_0 < 0$  to get  $a^* > 0$ ), the fastest-growing mode is localized and achieves a growth rate larger than  $\Gamma_0$ . The required curvature direction is in accord with the experiment, where the instability occurs at the dry fingertips ([11] and Fig. 1). Note that  $\epsilon = (q_1 a)^{-1} \sim |\kappa_0 \sigma| / (q_1 w) \ll 1$ , and  $\Gamma_{\max} / \Gamma_0 - 1 \sim \epsilon^2 \ll 1$ , which is consistent with the aforementioned approximations. The main result, Eq. (15), seems robust to the choice of trial function [20].

Two issues have remained unspecified in the discussion above. First, for our choice of  $\kappa(s)$   $\hat{O}$  is symmetric in  $\pm s$  and, therefore, the actual unstable mode must have a definite parity [i.e., the  $e^{iq_1s}$  factor in Eq. (11) should be replaced by either  $\cos(q_1s)$  or  $\sin(q_1s)$ ]. In the even case the perturbation is maximum at the tip, whereas in the odd case it has a node there. Within our approximation the difference in  $\bar{\Gamma}$  between the two functions is minute. If the overall turn is relatively small,  $|\kappa_0 \sigma| < \delta^{1/2}$ , we have  $a > \sigma$ , and the even perturbation is found to be slightly faster, with  $(\bar{\Gamma}_{\text{even}} - \bar{\Gamma}_{\text{odd}}) / \Gamma_0 = [8q_1^2\kappa_0^4\sigma^6 / (q_0^4w^4)] e^{-q_1^2\sigma^2}$ . An example of an even unstable mode is shown in Fig. 3. In the opposite case of  $|\kappa_0 \sigma| > \delta^{1/2}$  we have  $a < \sigma$ , and the growth rate of the odd perturbation is slightly higher,  $(\bar{\Gamma}_{\text{odd}} - \bar{\Gamma}_{\text{even}}) / \Gamma_0 = 2(q_1/q_0)^4 e^{-q_1^2 a^2/2}$ .

The second question concerns the sign of the localized instability — whether it increases the liquid height at  $s = 0$  toward the formation of a droplet, or decreases it toward pinch-off. A rigorous answer requires nonlinear analysis that lies beyond the scope of the current work. Yet, since the entire liquid film is unstable against evaporation, it is plausible to expect that the rim should shrink at its tip. This is also the direction required to account for the experimentally observed doublon patterns (Fig. 1). By Darcy's law the velocity of the interface increases with the local film height. Hence, a local indentation at the tip of a dry finger advances more slowly than its shoulders, leading to the shape of a finger split in two by a narrow liquid spine.

This work has two direct experimental implications. The first relates to the stable radial growth of domains, found in the dewetting of nonvolatile liquid films [2, 8, 9], vs. the unstable pattern formation observed in the evaporation of volatile ones [10–13]. We have shown that the qualitatively different dynamics in these two types of experiment can be related to the stability vs. instability of the accumulated liquid rim at the domain boundary. The second implication concerns the mechanism behind the patterns selected in the evaporation process. The newly demonstrated effect — a localized Rayleigh instability driven by the surface tension of a nonuniformly curved

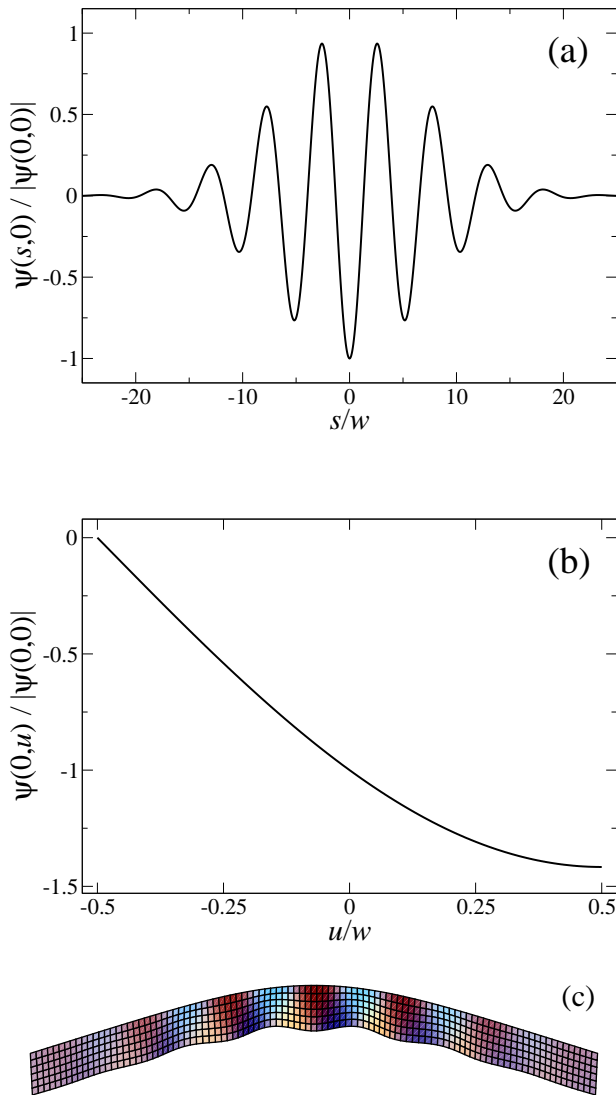


FIG. 3: Localized instability of a curved liquid rim. (a) Longitudinal profile of the height perturbation along the centerline,  $\psi(s,0)$ . (b) Transverse profile at the tip,  $\psi(0,u)$ . (c) (color online). Two-dimensional topography,  $\psi(s,u)$ . The parameters used are  $\kappa_0/w = -0.02$ ,  $\sigma/w = 7$ , and  $q_0w = 2$ .

liquid domain — is essential for the pattern formation as it suppresses the Saffman-Taylor instability at the finger tips. More broadly, since the relation between inhomogeneity and localization is far more general (encountered, e.g., in the effect of defects on electron states in a solid), we expect related localization effects to emerge in other scenarios of the Rayleigh instability. Indicating these scenarios calls for further investigation. Such localized

instabilities, for example, may offer new possibilities to control via curvature the precise location where a liquid filament is to agglomerate into a drop or pinch off.

We thank Yossi Avron, Eldad Bettelheim, Michael Elbaum, Steve Lipson, and Rachel Yerushalmi-Rozen for helpful discussions, and Tom Witten for valuable comments on the manuscript. HD wishes to thank the Racah Institute of Physics, Hebrew University, for its hospitality. This research has been supported in part by the Israel Science Foundation (ISF) under Grant Nos. 588/06 and 9/09.

\* Electronic address: agam@phys.huji.ac.il

- [1] J. Eggers, Rev. Mod. Phys. **69**, 865 (1997).
- [2] P.-G. de Gennes, F. Brochard-Wyart, and D. Quéré, *Capillarity and Wetting Phenomena*, Springer, 2004.
- [3] R. Bar-Ziv, E. Moses, and P. Nelson, Biophys. J. **75**, 294 (1998).
- [4] T. R. Powers and R. E. Goldstein, Phys. Rev. Lett. **78**, 2555 (1997). T. R. Powers, D. Zhang, R. E. Goldstein, and H. A. Stone, Phys. Fluids **10**, 1052 (1998).
- [5] R. C. T. da Costa, Phys. Rev. A **23**, 1982 (1981); **25**, 2893 (1982).
- [6] P. Exner and P. Seba, J. Math. Phys. **30**, 2574 (1989).
- [7] D. Bonn, J. Eggers, J. Indekeu, J. Meunier, and E. Rolley, Rev. Mod. Phys. **81**, 739 (2009).
- [8] C. Redon, F. Brochard-Wyart, and F. Rondelez, Phys. Rev. Lett. **66**, 715 (1991).
- [9] R. Seemann, S. Herminghaus, and K. Jacobs, Phys. Rev. Lett. **86**, 5534 (2001).
- [10] M. Elbaum and S. G. Lipson, Phys. Rev. Lett. **72**, 3562 (1994).
- [11] N. Samid-Merzel, S. G. Lipson, and D. S. Tannhauser, Phys. Rev. E **57**, 2906 (1998).
- [12] I. Leizerson, S. G. Lipson, and A. V. Lyushnin, Nature **422**, 395 (2003).
- [13] I. Leizerson, S. G. Lipson, and A. V. Lyushnin, Langmuir **20**, 291 (2004).
- [14] X. Gu, D. Raghavan, J. F. Douglas, and A. Karim, J. Polym. Sci. B: Polym. Phys. **40**, 2825 (2002).
- [15] O. Agam, Phys. Rev. E **79**, 021603 (2009).
- [16] A. Oron, S. H. Davis, and S. G. Bankoff, Rev. Mod. Phys. **69**, 931 (1997).
- [17] The picture used in Fig. 1 is courtesy of S. G. Lipson.
- [18] The boundary condition (6) implies that, unlike other Rayleigh instabilities, the rim can exchange liquid with the film and its mass is not conserved.
- [19] One can treat  $q_1$  as another variational parameter, yet this does not significantly improve the results.
- [20] Identical results are obtained using a different trial function,  $\phi = \sin[k_1(u + w/2)]$  times a 3rd-order polynomial in  $u$ , whose coefficients are so chosen as to satisfy the boundary conditions (6) and (7) for fixed  $\kappa$ .